Supplement of Atmos. Chem. Phys., 20, 14669–14693, 2020
https://doi.org/10.5194/acp-20-14669-2020-supplement
© Author(s) 2020. This work is distributed under
the Creative Commons Attribution 4.0 License.

Atmospheric Chemistry and Physics
Open Access

Supplement of

Role of equatorial waves and convective gravity waves in the 2015/16 quasi-biennial oscillation disruption

Min-Jee Kang et al.

Correspondence to: Hye-Yeong Chun (chunhy@yonsei.ac.kr) and Min-Jee Kang (kangmj@yonsei.ac.kr)

The copyright of individual parts of the supplement might differ from the CC BY 4.0 License.

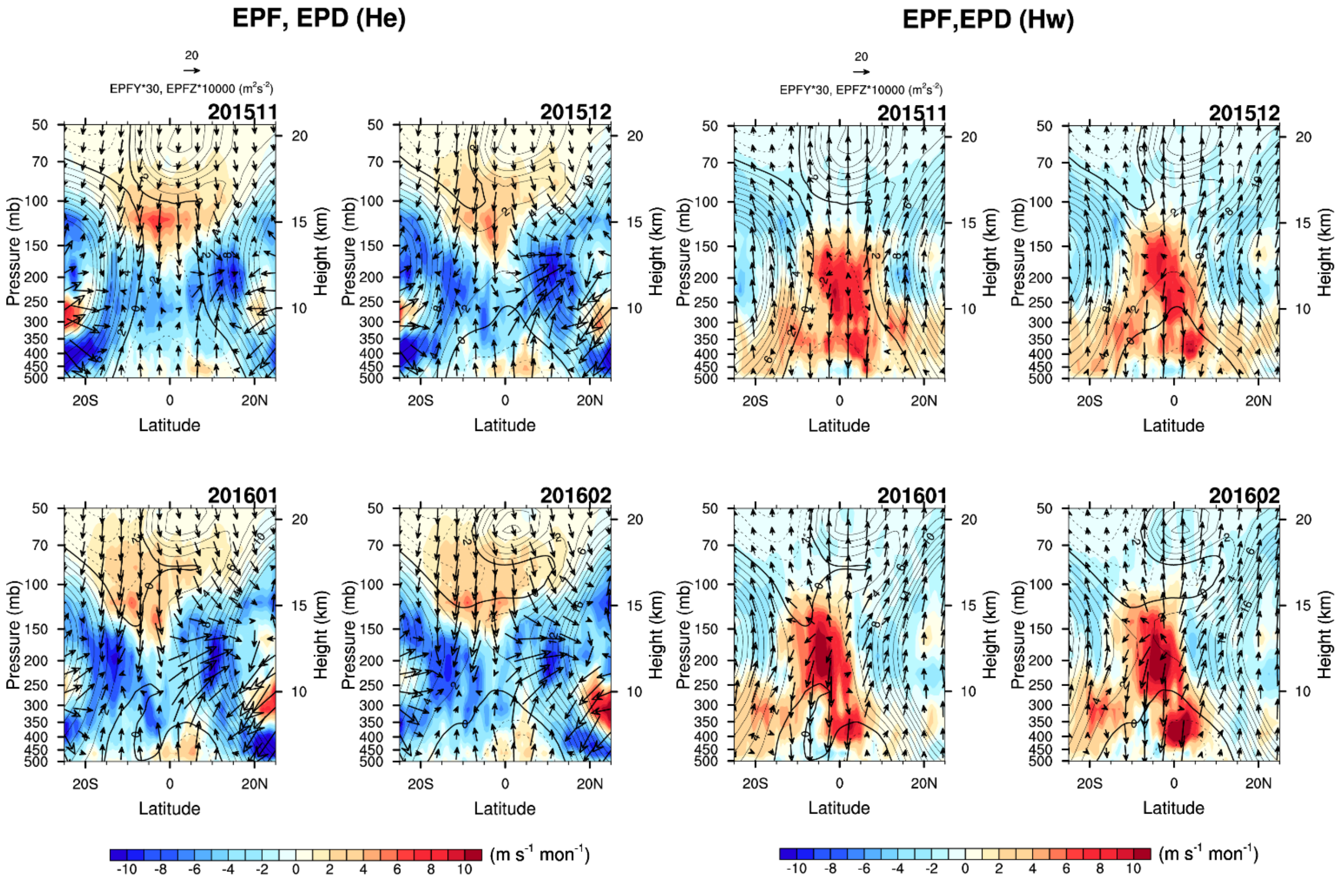

Figure S1. Latitude-height cross sections of EP flux (vectors) divided by air density and EP flux divergence (EPD, shading) for the H_e waves ($k > 20$ and $\omega > 0$ cpd or (ii) $0 < k \leq 20$ and $\omega > 0.4$ cpd) and H_w waves ($k <$ -20 and $\omega > 0$ cpd or (ii) -20 $\leq k < 0$ and $\omega > 0.4$ cpd) below 100 hPa and for the IG waves above 100 hPa from November 2015 to February 2016.

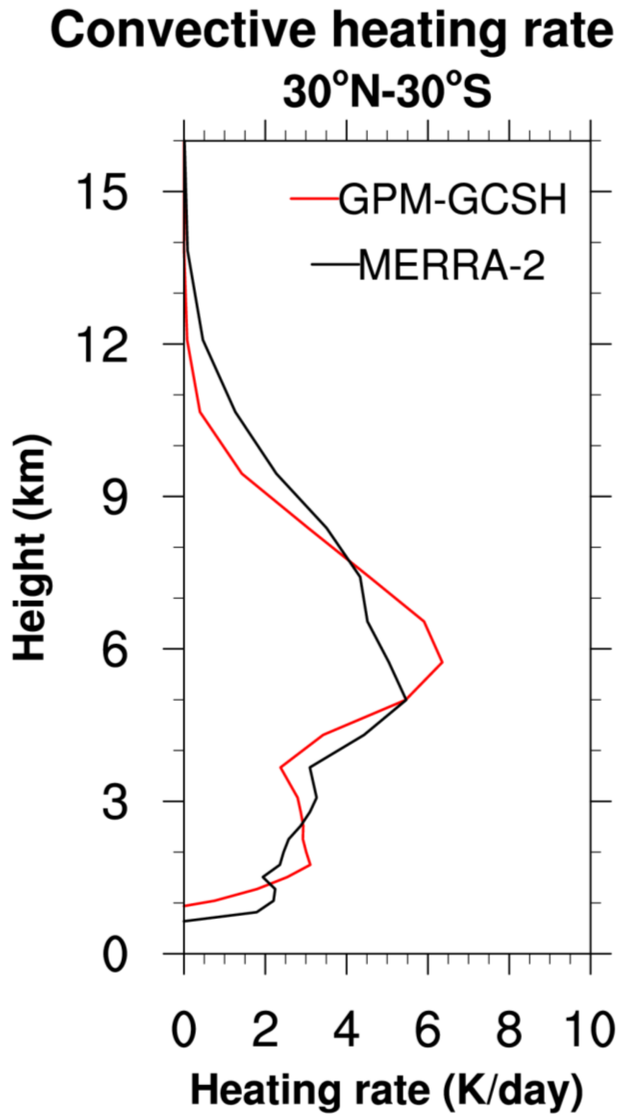

Figure S2. The vertical profiles of the convective heating rate given by the MERRA-2 data after applying criteria described in Sect. 2.4 (black) and those of the gridded convective stratiform heating (GCSH) estimated from Global Precipitation Measurement (GPM) observations (red) averaged over 30°N–30°S in February 2016. The comparison was made only when the GPM data exists and the MERRA-2 heating rate is nonzero. Note that the MERRA-2 heating rate is multiplied by a factor of 1.5 to focus on the shape of the profile because the magnitude of convective heating largely depends on the resolution provided. The overall difference in the magnitude of the convective heating rate can be adjusted by a conversion factor (c_f; Kang et al., 2017), a scale factor that constitutes convective source spectrum, when calculating the CGW momentum flux.

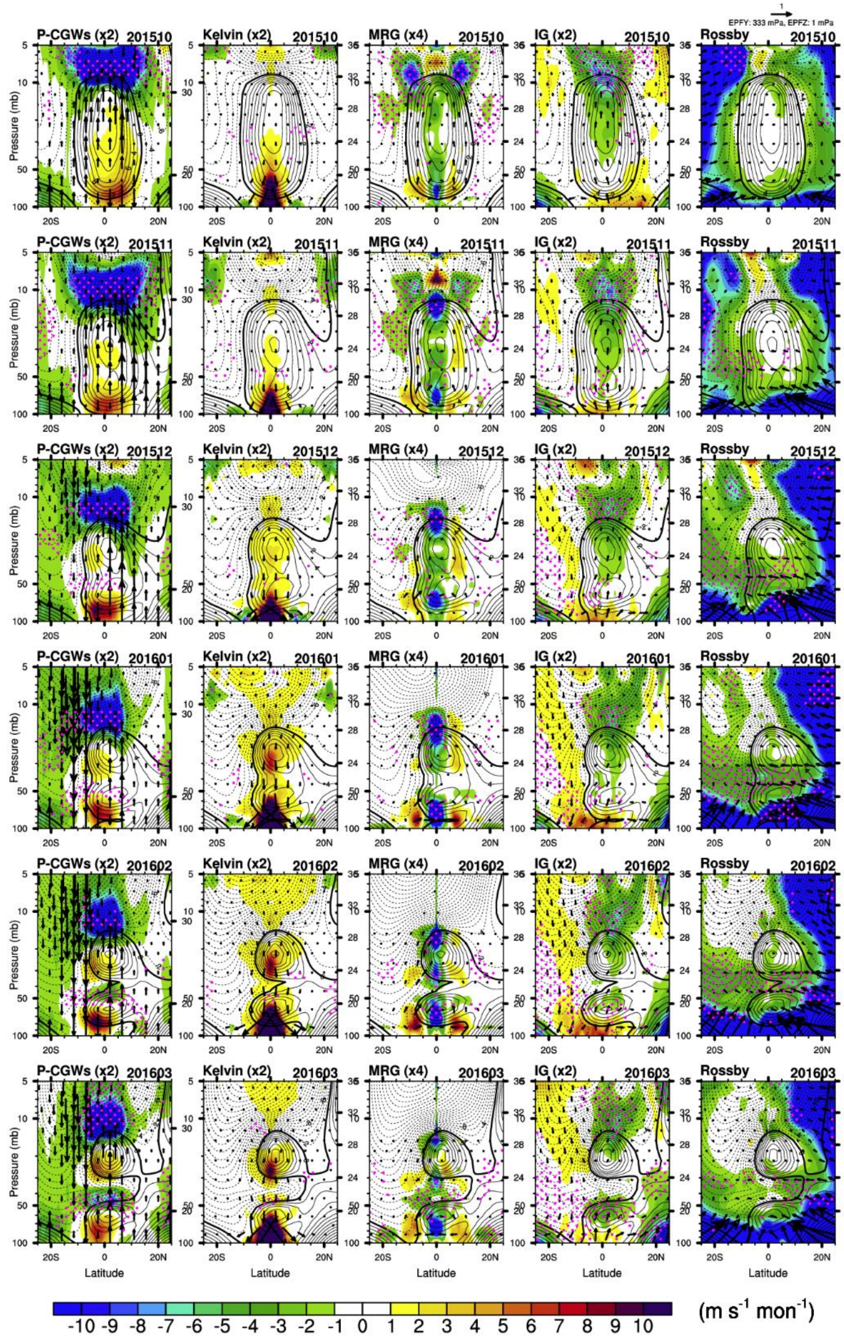

Figure S3. Latitude-height cross sections of the EP flux vectors and EP flux divergence (EPD) by parameterized CGWs (P-CGWs, multiplied by 2) and resolved equatorial waves, including Kelvin (multiplied by 2), MRG (multiplied by 4), inertia-gravity (IG, multiplied by 2), and Rossby waves from October 2015 to March 2016, superimposed with the zonal-mean zonal wind (contour lines). Positive (negative) zonal winds are plotted with solid (dashed) lines with a contour interval of 2 m s^{-1}, and thick contour lines denote a zero-zonal wind speed. The magenta-colored stippled pattern denotes a region where the EPD is smaller than the 1-standard deviation of WQBO climatology.

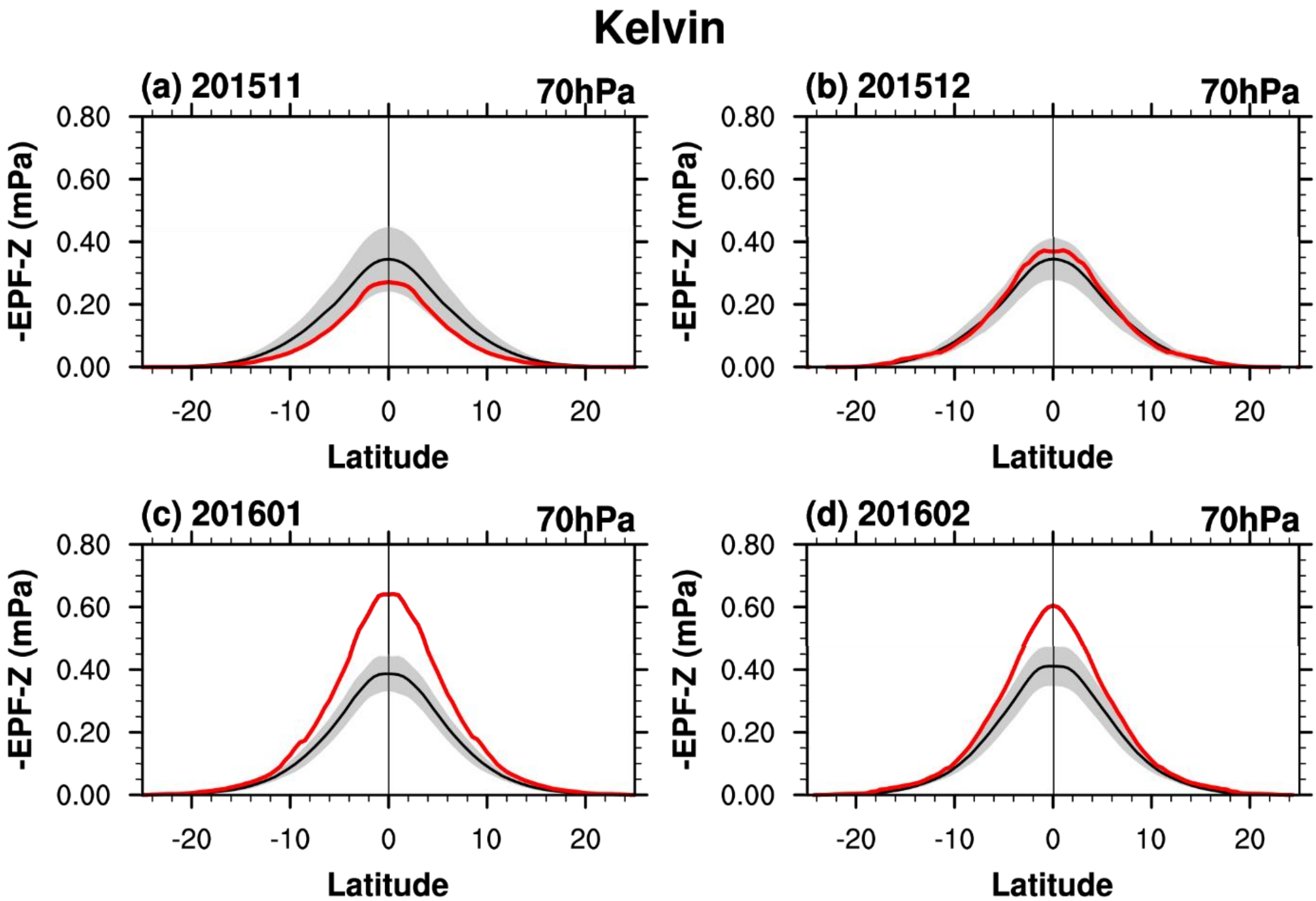

Figure S4. The magnitude of the vertical EP flux for the Kelvin waves at 70 hPa during the disruption (red): (a) November 2015, (b) December 2015, (c) January 2016, and (d) February 2016, and their monthly climatology for WQBO (black) along with ±1 standard deviation (gray shading).

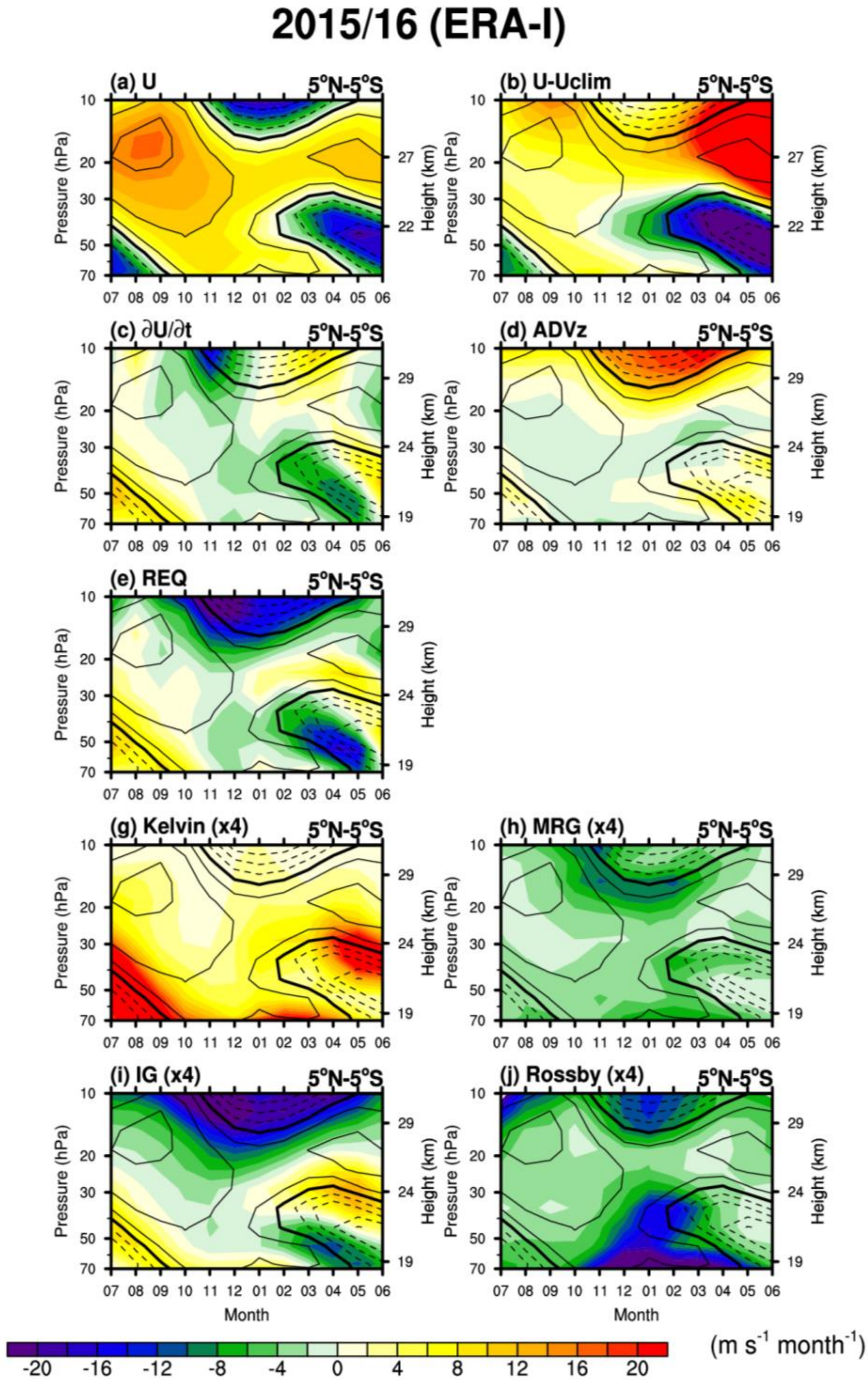

Figure S5. The same as in Fig. 3 but for the QBO disruption period exclusively using ERA-Interim data except for parameterized CGWD.

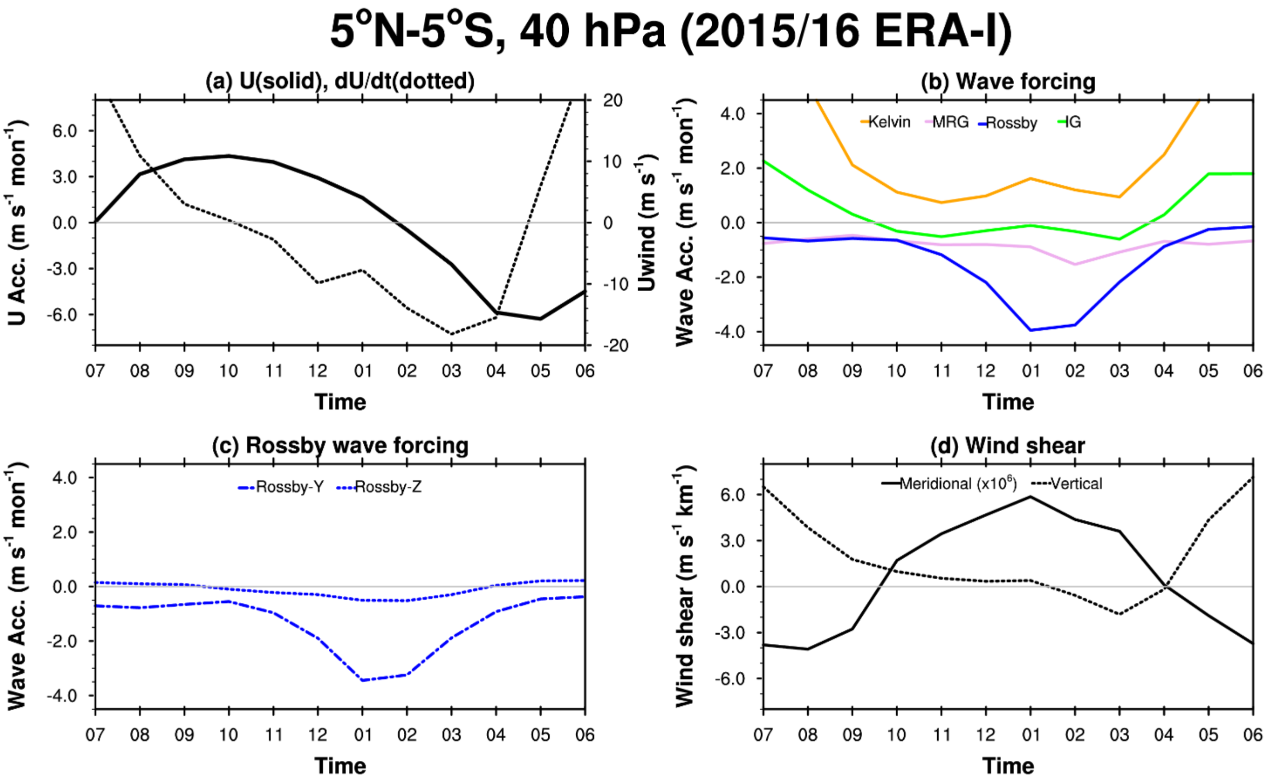

Figure S6. The same as in Fig. 4 but using ERA-Interim data except for parameterized CGWD.

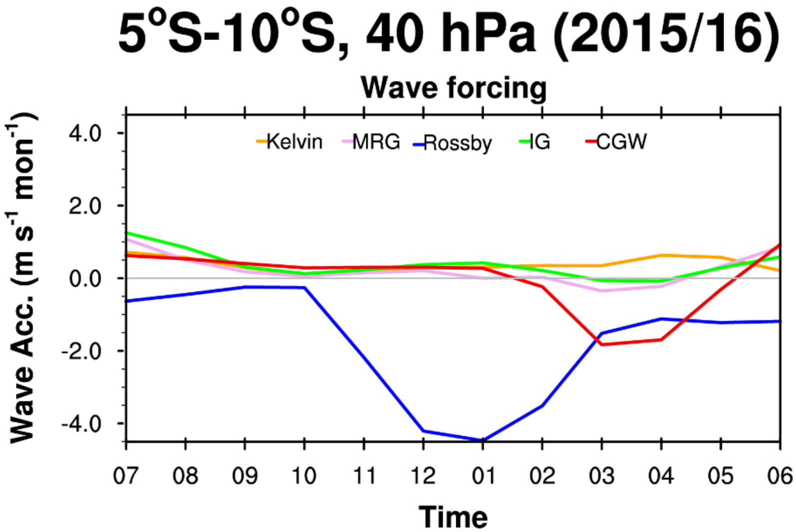

Figure S7. Time series of the wave forcing by the Kelvin waves (orange), MRG waves (pink), Rossby waves (blue), IG waves (light green), and CGWs (red) averaged over 5°S–10°S at 40 hPa from July 2015 to June 2016 using MERRA-2 data.

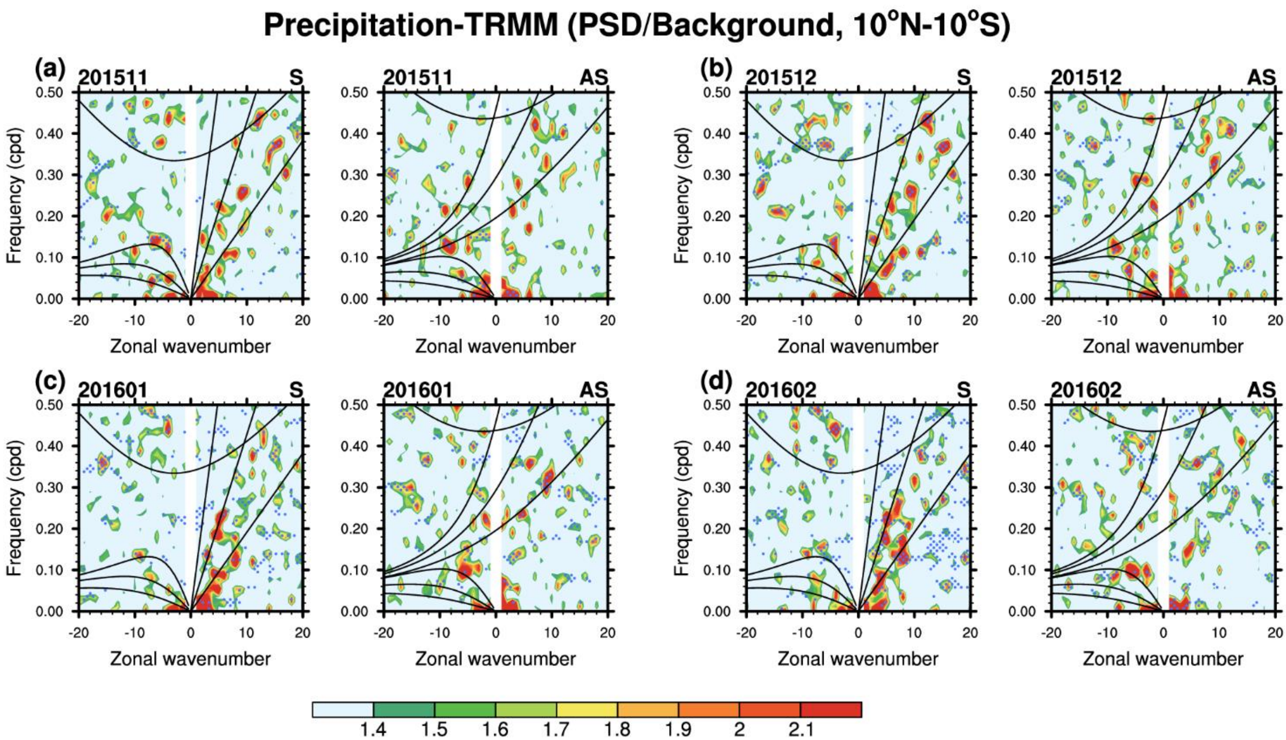

Figure S8. The same as in Fig. 10 but using TRMM 3B42 precipitation data. Note that TRMM data are available form 1998, so the WQBO climatology includes only five winters: 2013-2014, 2010-2011, 2008-2009, 2006-2007, 1999-2000. The ratio of 1.4 corresponds to a statistically significant spectrum at 99% level for TRMM (dof=82) because the horizontal resolution is 0.25°.

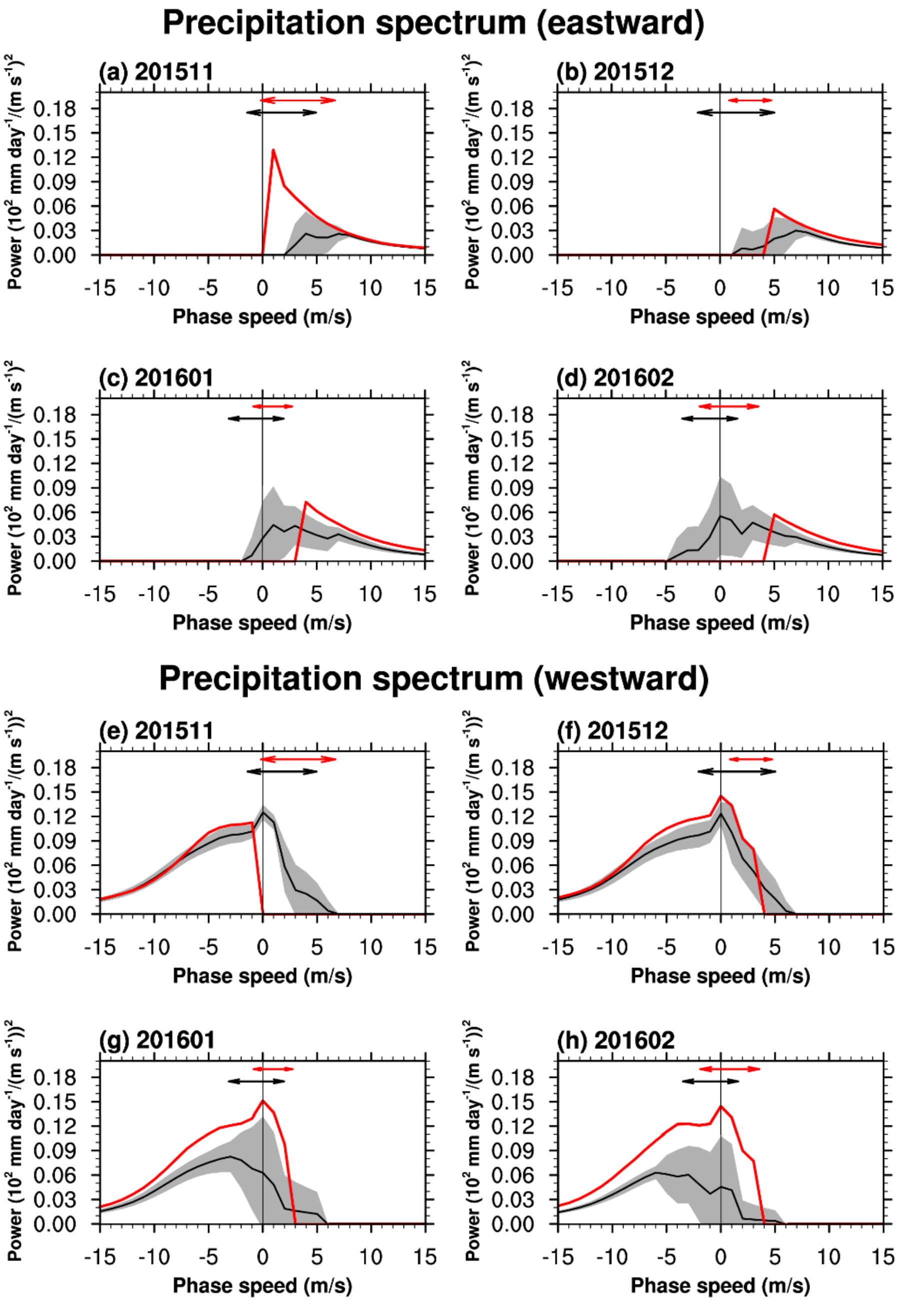

Figure S9. The same as Figure 13 but for eastward and westward waves, respectively. We assumed the source level as 140 hPa (Fig. S1; Sect. 2.3) and the spectrum where the phase speed is greater (smaller) than zonal wind at the source level is defined as eastward (westward) waves.